


Cite this: *RSC Adv.*, 2018, 8, 30387

# The influence of composition on the functionality of hybrid CuO–ZnO–Al<sub>2</sub>O<sub>3</sub>/HZSM-5 for the synthesis of DME from CO<sub>2</sub> hydrogenation

Yubing Hu, Yajing Zhang, \* Jie Du, Chunyan Li, Kangjun Wang,\* Lidong Liu, Xinrui Yu, Kai Wang and Nan Liu

A series of CuO–ZnO–Al<sub>2</sub>O<sub>3</sub>/HZSM-5 hybrid catalysts with different Cu/Zn ratios and disparate Al<sub>2</sub>O<sub>3</sub> doping were prepared and characterized by XRD, BET, H<sub>2</sub>-TPR, NH<sub>3</sub>-TPD and XPS techniques. The optimal Cu/Zn ratio is 7 : 3, and the introduction of a suitable amount of Al<sub>2</sub>O<sub>3</sub> to form hybrid catalysts increased the BET specific area and micropore volume, facilitated the CuO dispersion, decreased the CuO crystallite size, increased the interaction between CuO and ZnO, enhanced the number of weak acid sites, altered the copper chemical state and improved the catalytic performance consequently. The highest CO<sub>2</sub> conversion, DME selectivity and DME yield of 27.3%, 67.1% and 18.3%, respectively, were observed over the CZA<sub>7</sub>H catalyst. The suitable temperature of 260 °C and the appropriate space velocity of 1500 h<sup>−1</sup> for one-step synthesis of dimethyl ether (DME) from carbon dioxide (CO<sub>2</sub>) hydrogenation were also investigated. The 50 h stability of the CZA<sub>7</sub>H catalyst was also tested.

Received 6th June 2018  
Accepted 18th August 2018

DOI: 10.1039/c8ra04814b

rsc.li/rsc-advances

## 1. Introduction

CO<sub>2</sub> emission is increasing at an unparalleled rate due to fossil fuel combustion in recent years.<sup>1</sup> As a consequence, excessive CO<sub>2</sub> release leads to a series of problems such as global warming and environmental pollution.<sup>2,3</sup> Therefore, CO<sub>2</sub> recycling and utilization are very imperative.<sup>4,5</sup> CO<sub>2</sub> hydrogenation to dimethyl ether (DME) is an excellent option.<sup>6</sup>

DME is attracting more and more interest as a green fuel because it produces less CO<sub>x</sub>, NO<sub>x</sub>, and SO<sub>x</sub> particulates when combusted.<sup>7</sup> Therefore, DME is considered as a potential environmentally friendly alternative option to petrol diesel for diesel engines.<sup>8</sup> Meanwhile, DME, as a vital chemical intermediate, can also be used to prepare diversified valuable chemical products especially esters and lower olefins.<sup>9</sup> Furthermore, it can be utilized in several fields, for example, in fuel additives of diesel, home heating and cooking gas, and pro-environmental refrigerants.<sup>10,11</sup>

The hydrogenation of CO<sub>2</sub> to DME over a hybrid catalyst for DME synthesis is principally composed of three independent reactions, methanol synthesis from CO<sub>2</sub> hydrogenation (CO<sub>2</sub> + 3H<sub>2</sub> ↔ CH<sub>3</sub>OH + H<sub>2</sub>O reaction 1), methanol dehydration to form DME (2CH<sub>3</sub>OH ↔ CH<sub>3</sub>OCH<sub>3</sub> + H<sub>2</sub>O reaction 2), and a reverse water gas shift reaction (RWGS) (CO<sub>2</sub> + H<sub>2</sub> ↔ CO + H<sub>2</sub>O reaction 3). DME can be produced *via* a two-step process including reaction 1 on a copper based catalyst and subsequent

reaction 2 over a solid acid catalyst. Furthermore, one-step process (performing the two steps simultaneously over a hybrid catalyst) has a better performance as a thermodynamically favorable course because the equilibrium limitation of reaction 1 can be readily overcome by reaction 2.<sup>12,13</sup>

Currently, hybrid catalysts of methanol synthesis component and methanol dehydration component are applied to the one-step direct DME synthesis from CO<sub>2</sub>.<sup>14,15</sup> The methanol dehydration components are generally solid acid catalyst such as γ-Al<sub>2</sub>O<sub>3</sub>, but the active sites of the γ-Al<sub>2</sub>O<sub>3</sub> is Lewis acid sites which are favored for water adsorption, resulting in a significant reduction of the amount of acid sites and then a decrease of catalytic activity. Another intriguing solid acid catalyst is WO<sub>x</sub>/ZrO<sub>2</sub>, but the catalytic activity of WO<sub>x</sub>/ZrO<sub>2</sub> is lower due to its weaker acid strength present.<sup>16</sup> Besides, SAPO-18 has been used as acid function owing to its uniform microporous structure and a high stability, but SAPO-18 possesses a large number of moderate strength acid sites, which cause catalyst deactivation as well as undesired products by coke deposition.<sup>17</sup> By contrast, HZSM-5 is the most suitable acidic component due to its more hydrophobic character and advantage of Brønsted acidity, which significantly reduces the impact of water on HZSM-5.<sup>18–23</sup> Furthermore, HZSM-5 possesses weak acid sites which are in favor of methanol dehydration to DME at low temperatures and exhibits high catalytic activity.<sup>24</sup> However, the methanol synthesis components of the hybrid catalysts are various, and the Cu–Zn based catalyst is regarded as the most promising binary catalyst among them. Xiao *et al.* reported the deposition of Zn on the surface of copper can increase surface area and can form a unique site at the Cu–ZnO interface to improve the

College of Chemical Engineering, Shenyang University of Chemical Technology, Shenyang 110142, PR China. E-mail: yjzhang2009@163.com; angle\_79@163.com; Tel: +86-24-89383902



adsorption of CO<sub>2</sub> and catalyst activity.<sup>25,26</sup> To further improve the performance of the Cu–Zn bimetallic compound catalyst, adding an amphoteric metal oxide species as additive to Cu–Zn based catalyst is an efficient method. Al<sub>2</sub>O<sub>3</sub> is a prospective co-catalyst of sufficient attraction due to its mechanical and thermal stability, its excellent dispersion feature of copper and zinc. Nevertheless, only a few literatures have reported Al<sub>2</sub>O<sub>3</sub> as a single additive of the Cu–Zn based catalyst for one-step direct DME synthesis from CO<sub>2</sub> hydrogenation at present. Lei *et al.* studied hydrogenation of CO<sub>2</sub> to CH<sub>3</sub>OH over CuO–ZnO–Al<sub>2</sub>O<sub>3</sub> catalysts prepared *via* a solvent-free route, they found that the combustion processes and physicochemical properties of catalysts depend strongly on the type and amount of fuel.<sup>27</sup> Allahyari *et al.* reported CuO–ZnO–Al<sub>2</sub>O<sub>3</sub>/HZSM-5 nanocatalyst for direct synthesis DME as a green fuel from syngas, the catalysts were prepared by ultrasound-assisted co-precipitation method at different irradiation times, and the result revealed the relationship between irradiation time and catalytic performance.<sup>28</sup> Bowker *et al.* studied the mechanism of methanol synthesis on copper/zinc oxide/aluminum catalyst, and found that the energetics of formate hydrogenation/hydrogenolysis on the copper component of the catalyst was unaffected by the intimate mixing of copper and zinc oxide in the catalyst.<sup>29</sup> Liu reported preparation of HZSM-5 membrane packed CuO–ZnO–Al<sub>2</sub>O<sub>3</sub> nanoparticles for catalysing carbon dioxide hydrogenation to DME, they found zeolite capsule catalysts exhibited an excellent DME selectivity compared with the conventional hybrid catalyst because the further dehydration of DME was restrained.<sup>10</sup> Unfortunately, those above mentioned literature of CO<sub>2</sub> hydrogenation over CuO–ZnO–Al<sub>2</sub>O<sub>3</sub> catalyst were mainly related to the influence of catalyst preparation methods to the catalyst activity as well as the mechanism of CO<sub>2</sub> hydrogenation. On the contrary, the effect of the amount of the additive Al<sub>2</sub>O<sub>3</sub> of CuO–ZnO–Al<sub>2</sub>O<sub>3</sub> catalyst on catalyst activity was rarely investigated. Meanwhile, the Cu/Zn ratio of the CuO–ZnO–Al<sub>2</sub>O<sub>3</sub> catalyst currently still derived from methanol synthesis from CO<sub>2</sub> hydrogenation or from syngas hydrogenation.<sup>30</sup>

Here, we prepared a series of CuO–ZnO–Al<sub>2</sub>O<sub>3</sub>/HZSM-5 hybrid catalysts of different Al<sub>2</sub>O<sub>3</sub> contents by the oxalate co-precipitation method, on the basis of optimizing Cu/Zn ratio of catalyst for DME synthesis from CO<sub>2</sub> hydrogenation. The effect of Al<sub>2</sub>O<sub>3</sub> content on catalytic properties especially CO<sub>2</sub> conversion and DME selectivity of the hybrid catalysts was investigated. Moreover, the influence of reaction temperature and velocity on the catalyst activity of the hybrid catalyst with optimum Al<sub>2</sub>O<sub>3</sub> content was also investigated.

## 2. Experimental

### 2.1 Preparation of CuO–ZnO/HZSM-5 catalysts

A series of CuO–ZnO/HZSM-5 catalysts of diverse Cu/Zn molar ratio were prepared, aiming at confirming optimum composition. Cu(NO<sub>3</sub>)<sub>2</sub>·3H<sub>2</sub>O, Zn(NO<sub>3</sub>)<sub>2</sub>·6H<sub>2</sub>O (Cu/Zn molar ratio ranging from 2 : 8 to 8 : 2) were dissolved in ethanol to gain the metal nitrates solution and coprecipitated by oxalate under vigorous stirring at 60 °C in a solution containing the HZSM-5 finely dispersed, with a final CuO–ZnO : HZSM-5 weight ratio

of 2 : 1, for convenience of comparison with previous work.<sup>7,31,32</sup> The HZSM-5 with a SiO<sub>2</sub>/Al<sub>2</sub>O<sub>3</sub> ratio of 38 was purchased from Catalyst Plant of Nankai University (China). The slurry was heated to 80 °C and was aged for 2 h under stirring. Subsequently, the slurry was evaporated at the same temperature. Then the obtained product was dried in muffle furnace at 120 °C for 12 h and calcined in air at 400 °C for 4 h. The final product was hybrid catalyst named as C<sub>x</sub>Z<sub>10–x</sub>H (the *x* express the molar ratio of CuO : CuO–ZnO) and was pressed, crushed and griddled to get the granules (20–40 mesh).

### 2.2 Preparation of CuO–ZnO–Al<sub>2</sub>O<sub>3</sub>/HZSM-5 hybrid catalysts

Thereafter, a series of CuO–ZnO–Al<sub>2</sub>O<sub>3</sub>/HZSM-5 hybrid catalysts of different Al<sub>2</sub>O<sub>3</sub> contents were prepared. Cu(NO<sub>3</sub>)<sub>2</sub>·3H<sub>2</sub>O, Zn(NO<sub>3</sub>)<sub>2</sub>·6H<sub>2</sub>O were weighed according to the optimal Cu/Zn mole ratio which was determined in the preliminary experiments. The mixture was dissolved in ethanol followed by the addition of Al(NO<sub>3</sub>)<sub>3</sub>·9H<sub>2</sub>O. The amount of the Al(NO<sub>3</sub>)<sub>3</sub>·9H<sub>2</sub>O used depended on the required Al<sub>2</sub>O<sub>3</sub> contents of 0, 1.0, 3.0, 5.0, 7.0, 10.0 wt% in CuO–ZnO–Al<sub>2</sub>O<sub>3</sub>. Then, the solution of precursors was added to a vigorously stirred ethanol solution containing the oxalic acid and the powdered HZSM-5 in a constant and slow manner at 60 °C. The weight ratio of the final oxide of CuO–ZnO–Al<sub>2</sub>O<sub>3</sub> to HZSM-5 is 2 : 1. The slurry was dealt with the same procedure as the C<sub>x</sub>Z<sub>10–x</sub>H and the final product was abbreviated as CZA<sub>y</sub>H, where the *y* represents theoretical Al<sub>2</sub>O<sub>3</sub> : CuO–ZnO–Al<sub>2</sub>O<sub>3</sub> wt%.

### 2.3 Catalyst testing

The hybrid catalyst activity was measured in a continuous-flow fixed-bed reactor made of stainless steel (10 mm inner diameter). 1 mL of the hybrid catalyst was diluted with 0.5 mL of the quartz sand (both in 20–40 mesh). Prior to the test, the catalyst was reduced *in situ* in a stream of 10% H<sub>2</sub>/N<sub>2</sub> at 300 °C for 3 h under atmospheric pressure. After the reduction, the reactor was cooled to room temperature under flowing N<sub>2</sub> and reactant gas flow (H<sub>2</sub>/CO<sub>2</sub>/N<sub>2</sub> = 3/9/1, molar) was introduced, subsequently raising the pressure to 3.0 MPa and the reaction temperature was raised to 260 °C. Analysis of the products were performed applied a gas chromatograph (SP2100A) equipped with both a TCD (for N<sub>2</sub>, CO and CO<sub>2</sub>, GDX-101 connected with Porapak T column) and a FID (for CH<sub>4</sub>, CH<sub>3</sub>OH and DME, Porapak Q column). The CO<sub>2</sub> conversion as well as the selectivity toward CO, CH<sub>3</sub>OH and DME are calculated by internal standard method.<sup>32,33</sup> X<sub>CO<sub>2</sub></sub>, S<sub>P</sub> and Y<sub>DME</sub> represent the conversion of CO<sub>2</sub>, the selectivity of the product (DME, MeOH, CO) and the yield of DME, respectively. Each experimental data was corresponds to an average of three independent measurements, with error of ±2%.

$$X_{\text{CO}_2} = \frac{\text{CO}_{2,\text{in}}/\text{N}_{2,\text{in}} - \text{CO}_{2,\text{out}}/\text{N}_{2,\text{out}}}{\text{CO}_{2,\text{in}}/\text{N}_{2,\text{in}}} \quad (1)$$

$$S_{P_i} = \frac{P_i}{1 - \text{CO}_{2,\text{out}}} \quad (2)$$



where  $P_i$  stands for the concentration of a specific product (DME, MeOH, CO).

$$Y_{\text{DME}} = S_{\text{DME}} X_{\text{CO}_2} \quad (3)$$

## 2.4 Catalyst characterization

X-ray powder diffraction (XRD) patterns of all samples were performed on a Rigaku D/max 2500 pc X-ray diffractometer with Cu-K $\alpha$  radiation ( $\lambda = 1.54156 \text{ \AA}$ ) at a scan rate of  $4^\circ \text{ min}^{-1}$  at 50 kV and 250 mA.

The BET surface area of the samples were conducted by N<sub>2</sub> adsorption at  $-196^\circ \text{C}$  using a Quantachrome Autosorb 1-C. Before the absorption-desorption measurements, samples were degassed under vacuum at  $300^\circ \text{C}$  for 3 h. The specific BET ( $S_{\text{BET}}$ ) was estimated from the linear part of the Brunauer-Emmett-Teller (BET) plot.

The X-ray photoelectron spectroscopy (XPS) and X-ray-induced Auger electron spectroscopy were recorded on an ESCALA 250 Xi spectrometer, using a standard Al-K $\alpha$  X-ray source (1486.6 eV). The binding energy (BE) values were referenced to the adventitious C 1s peak (284.6 eV). Quantification of the surface atomic concentrations was carried out using the sensitivity factors supplied for the XPS instrument.

H<sub>2</sub>-TPR of catalysts were performed on chemisorptions (ChemBET 3000). Before reduction, 0.02 g of sample was pre-heated with flowing He at  $400^\circ \text{C}$  for 60 min, then cooled down room temperature. Subsequently, the temperature was raised in 10% H<sub>2</sub>/Ar ( $50 \text{ mL min}^{-1}$ ) at a ramp rate of  $10^\circ \text{C min}$  to  $400^\circ \text{C}$ . H<sub>2</sub> consumption was detected by TCD.

NH<sub>3</sub>-TPD of the samples were measured on the same apparatus for H<sub>2</sub>-TPR measurements. 0.1 g sample was heated to  $400^\circ \text{C}$  and maintained for 30 min, then the temperature was cooled to  $100^\circ \text{C}$ . After that, a 6 vol% NH<sub>3</sub>/Ar mixture stream was introduced to the sample for 60 min. Then, the examined sample was flushed with helium stream ( $30 \text{ mL min}^{-1}$ ) for 60 min to remove the weak adsorbed NH<sub>3</sub>. The temperature was raised from  $100^\circ \text{C}$  to  $800^\circ \text{C}$  at a rate of  $10^\circ \text{C min}$ .

## 3. Results and discussion

### 3.1 The effect of the Cu/Zn molar ratio on the catalytic performance of C<sub>x</sub>Z<sub>10-x</sub>H catalysts

In order to investigate the optimal Cu/Zn molar ratio of the hybrid catalysts, a series of C<sub>x</sub>Z<sub>10-x</sub>H catalysts were prepared. The catalytic performances of catalysts with different Cu/Zn molar ratio were summarized in Table 1. The CO<sub>2</sub> conversion, DME selectivity and the yield of DME increased with the Cu/Zn increased from 2 : 8 to 7 : 3, and decreased if continue raising the Cu/Zn to 8 : 2. The C<sub>7</sub>Z<sub>3</sub>H exhibited the maximum CO<sub>2</sub> conversion, DME selectivity and DME yield values of 19.2%, 47.8% and 9.2%, respectively. The result revealed the Cu/Zn molar ratio can affect the catalytic performance and the optimal Cu/Zn molar ratio of the hybrid catalysts was 7 : 3.

Table 1 Catalytic performance of the C<sub>x</sub>Z<sub>10-x</sub>H Hybrid catalysts<sup>a</sup>

Catalyst	Conversion of CO <sub>2</sub> /%	Selectivity/%				Yield/% DME
		DME	CH <sub>3</sub> OH	CO	Hydrocarbons	
C <sub>2</sub> Z <sub>8</sub> H	16.06	25.41	5.34	67.35	1.90	4.08
C <sub>3</sub> Z <sub>7</sub> H	16.44	27.04	8.03	63.14	1.79	4.45
C <sub>4</sub> Z <sub>6</sub> H	17.71	36.71	5.23	56.16	1.90	6.50
C <sub>5</sub> Z <sub>5</sub> H	17.46	37.73	5.22	55.22	1.83	6.59
C <sub>6</sub> Z <sub>4</sub> H	18.06	38.42	6.01	53.70	1.87	6.94
C <sub>7</sub> Z <sub>3</sub> H	19.20	47.80	1.70	47.80	2.70	9.20
C <sub>8</sub> Z <sub>2</sub> H	18.16	39.35	5.15	53.49	2.01	7.15

<sup>a</sup> Reaction conditions:  $T = 260^\circ \text{C}$ ;  $P = 3.0 \text{ MPa}$ ; CO<sub>2</sub> : H<sub>2</sub> : N<sub>2</sub> = 3 : 9 : 1; GHSV =  $1500 \text{ h}^{-1}$ .

### 3.2 Catalytic performance of the CZA<sub>y</sub>H catalysts

The catalytic performances of the CZA<sub>y</sub>H catalysts with different Al<sub>2</sub>O<sub>3</sub> contents were listed in Table 2. DME was the major product and the by products included CO and methanol under the reaction temperature of  $260^\circ \text{C}$ , pressure of 3.0 MPa and GHSV of  $1500 \text{ h}^{-1}$ . Moreover, several hydrocarbons such as CH<sub>4</sub> were also detected. The catalytic performances of the Al<sub>2</sub>O<sub>3</sub>-modified hybrid catalysts were enhanced enormously compared with the Al<sub>2</sub>O<sub>3</sub>-free hybrid catalyst. With the Al<sub>2</sub>O<sub>3</sub> contents increase in the catalysts (range from CZA<sub>0</sub>H to CZA<sub>7</sub>H), the CO<sub>2</sub> conversion, DME selectivity and the DME yield increased significantly. Further increasing the contents of Al<sub>2</sub>O<sub>3</sub> (CZA<sub>10</sub>H) decreased the catalysts activity. The CZA<sub>7</sub>H catalyst exhibited the highest catalyst performance and a maximum CO<sub>2</sub> conversion of 27.3% with a DME selectivity of 67.1% and a yield of DME of 18.3%, as shown in Table 2. The DME yield and the DME selectivity of CZA<sub>7</sub>H catalyst were appreciable in comparison of nearly 13.5% and 63.4%, respectively, obtained over CuO-ZnO-ZrO<sub>2</sub>/HZSM-5 catalyst reported by Li *et al.*<sup>34</sup> Meanwhile, the DME selectivity of 67.1% for CZA<sub>7</sub>H catalyst was significantly higher than 49.2% observed over CuO-ZnO-Al<sub>2</sub>O<sub>3</sub>/HZSM-5 catalyst studied by Zhang *et al.*<sup>31</sup> These results indicated suitable Al<sub>2</sub>O<sub>3</sub> additive can improve the catalyst performance significantly.

Fig. 1 shows the effect of reaction temperature on the catalytic performance of CZA<sub>7</sub>H catalyst. It can be found that volcanic shape change trends of the CO<sub>2</sub> conversion, DME selectivity and the yield of DME *versus* the variation of the

Table 2 Catalytic performance of the CZA<sub>y</sub>H hybrid catalysts<sup>a</sup>

Catalyst	Conversion of CO <sub>2</sub> /%	Selectivity/%				Yield/% DME
		DME	CH <sub>3</sub> OH	CO	Hydrocarbons	
CZA <sub>0</sub> H	19.2	47.8	1.7	47.8	2.7	9.2
CZA <sub>1</sub> H	23.6	60.6	2.0	34.6	2.8	14.3
CZA <sub>3</sub> H	22.9	61.6	2.6	33.1	2.7	14.1
CZA <sub>5</sub> H	23.0	64.3	5.5	26.5	3.7	14.8
CZA <sub>7</sub> H	27.3	67.1	3.9	25.5	3.5	18.3
CZA <sub>10</sub> H	22.6	60.9	3.6	32.7	2.8	13.8

<sup>a</sup> Reaction conditions:  $T = 260^\circ \text{C}$ ;  $P = 3.0 \text{ MPa}$ ; CO<sub>2</sub> : H<sub>2</sub> : N<sub>2</sub> = 3 : 9 : 1; GHSV =  $1500 \text{ h}^{-1}$ .



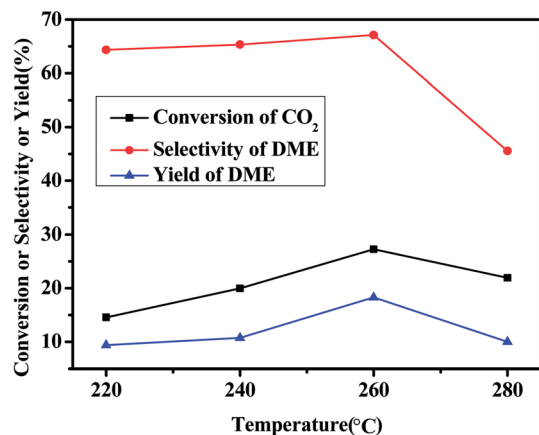


Fig. 1 Effect of temperature on catalytic CO<sub>2</sub> hydrogenation to DME for CZA<sub>7</sub>H hybrid catalysts.

temperature. With the temperature rising from 220 °C to 260 °C, the conversion of CO<sub>2</sub>, the selectivity of the DME and the DME yield increased obviously 12.7%, 2.7% and 8.9%, respectively, and then reduced sharply when the reaction temperature reached 280 °C. Comparing the catalytic performance data at several reaction temperatures, the optimal catalytic performance for the CZA<sub>7</sub>H catalyst were obtained at 260 °C. These results can be explained by the hydrogenation of CO<sub>2</sub> for synthesis of DME was a reversible exothermic reaction, the reverse reaction favored with an excessive temperature. Meanwhile, the main side reaction RWGS was an endothermic reaction thus the CO selectivity increased and the selectivity and yield of DME decreased with the reaction temperature higher than 260 °C.<sup>5</sup> In addition, the CZA<sub>7</sub>H catalyst activity may also decrease due to the Cu sintered and crystallized gradually with the reaction temperature increased.<sup>18</sup>

Fig. 2 illustrates the influence of the space velocity of on the catalytic performance of the CZA<sub>7</sub>H catalyst. It can be found that the CO<sub>2</sub> conversion, the DME selectivity and the DME yield decreased continuously from 27.3% to 20.5%, 67.1% to 52.3% and 18.3% to 10.7%, respectively, as the space velocity increased from 1500 to 3000 h<sup>-1</sup>. With the space velocity increasing, the

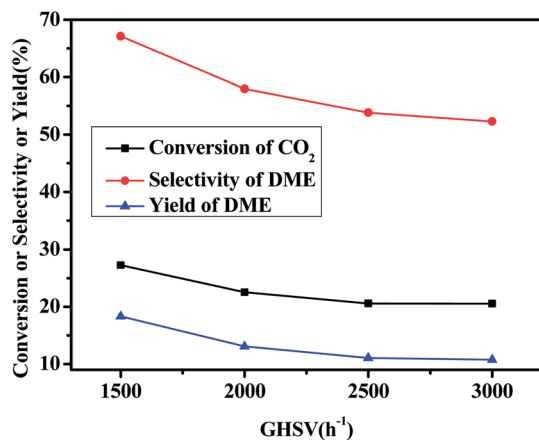


Fig. 2 Effect of space velocity on catalytic CO<sub>2</sub> hydrogenation to DME for CZA<sub>7</sub>H hybrid catalysts.

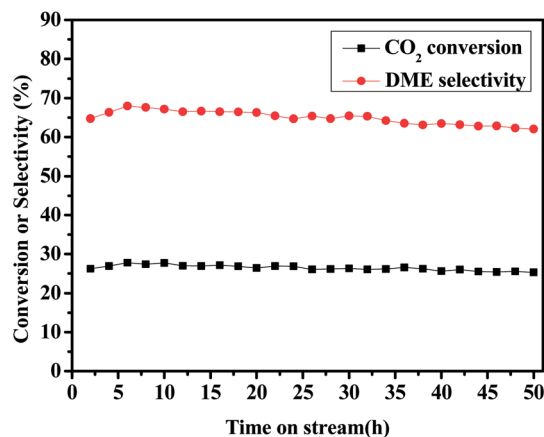


Fig. 3 Effects of the conversion of CO<sub>2</sub> and the selectivity of DME with CZA<sub>7</sub>H hybrid catalysts with time on stream.

contact time between reactants and the catalyst becomes short, consequently both the CO<sub>2</sub> hydrogenation to methanol and methanol dehydration to DME reactions could not proceed sufficiently.<sup>18</sup> Therefore, the conversion of CO<sub>2</sub> and the selectivity of the DME reduced distinctly indicating the efficient effect the space velocity on the catalytic performance.

### 3.3 Stability of the CZA<sub>7</sub>H catalyst

The stability of CZA<sub>7</sub>H catalyst was studied for the reaction of DME synthesis *via* CO<sub>2</sub> hydrogenation at 260 °C and 3.0 MPa with GHSV = 1500 h<sup>-1</sup>. The stability results were recorded every 2 h, as shown in Fig. 3. It can be found that the CO<sub>2</sub> conversion of and the DME selectivity decrease slightly from 27.3% and 67.1% to 25.3% and 62.1% during the continuous 50 h reaction process, respectively. The result indicated that the CZA<sub>7</sub>H catalyst possessed better catalytic performance and stability.

### 3.4 The structure of the catalysts

Fig. 4 illustrates the XRD patterns of a series of CZA<sub>x</sub>H catalysts with different Al<sub>2</sub>O<sub>3</sub> contents before H<sub>2</sub> reduction. For all catalysts, the diffraction peaks at  $2\theta = 35.5^\circ, 38.7^\circ, 48.7^\circ, 53.4^\circ, 58.2^\circ, 61.5^\circ, 66.2^\circ, 72.3^\circ$  and  $74.9^\circ$  can be ascribed to CuO phase (JCPDS no. 48-1548), the peaks at  $2\theta = 31.7^\circ, 34.3^\circ, 36.1^\circ, 47.4^\circ, 56.5^\circ, 62.8^\circ$  and  $67.8^\circ$  can be attributed to ZnO phase (JCPDS no. 65-3411), and the peaks appear in the  $2\theta$  range of  $21\text{--}25^\circ$  can be matched to HZSM-5 (JCPDS no. 44-0003). The peaks corresponding to Al<sub>2</sub>O<sub>3</sub> phase cannot be observed, indicating that the presence of Al<sub>2</sub>O<sub>3</sub> were amorphous phase or highly dispersed in the catalyst body phase. Compared with the peaks of catalyst CZA<sub>0</sub>H, the peaks of catalysts with Al<sub>2</sub>O<sub>3</sub> become weaker, indicating the CuO–ZnO oxides possess less intensive crystallinity. The diffraction peaks of CuO and ZnO weakened and broadened gradually with the increasing of Al<sub>2</sub>O<sub>3</sub> contents, even some diffraction peaks of CuO and ZnO phase disappeared, suggesting the decrease of grain size. The grain sizes of CuO ( $d_{\text{CuO}}$ ) and ZnO ( $d_{\text{ZnO}}$ ) for CZA<sub>x</sub>H catalysts calculated by Scherrer's equation are listed in Table 3. These results indicated obviously that the additive of Al<sub>2</sub>O<sub>3</sub> can improve the CuO dispersion and





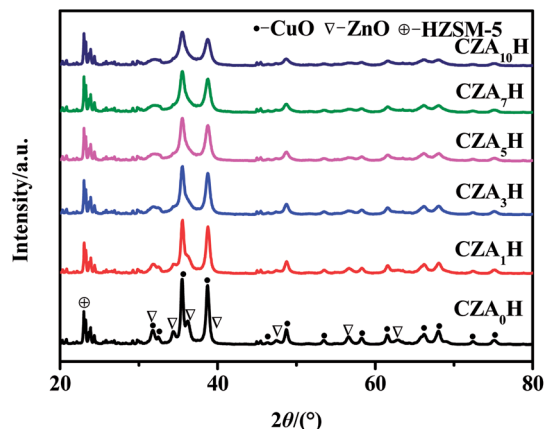


Fig. 4 XRD patterns of the CZA<sub>y</sub>H hybrid catalysts.

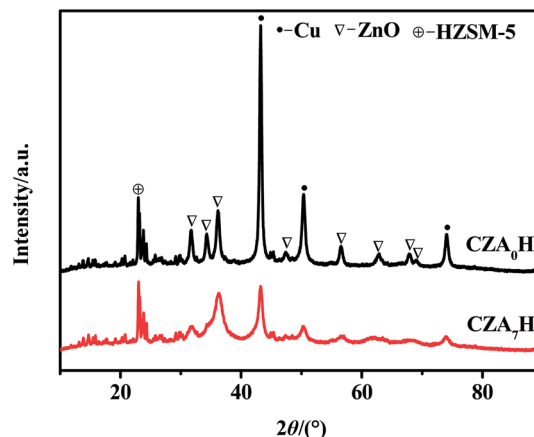


Fig. 5 XRD patterns of the reduced CZA<sub>0</sub>H and CZA<sub>7</sub>H hybrid catalysts.

can decrease the grain size of CuO. For all catalysts, the grain size of ZnO phase is greater than that of CuO phase, indicating ZnO phase closely relates to CuO phase. Shimokawabe *et al.* considered the grain size of ZnO is larger than CuO due to CuO can be well dissolved on the ZnO particles.<sup>35</sup> As a consequence, the active interface increased with the improving the dispersion of CuO.<sup>35,36</sup> Fig. 5 shows the XRD patterns of the reduced CZA<sub>0</sub>H and CZA<sub>7</sub>H catalysts. For these two catalysts, the diffraction peaks at  $2\theta = 43.3^\circ$ ,  $50.4^\circ$  and  $74.1^\circ$  can be ascribed to metallic copper phase (JCPDS no. 04-0836). No diffraction peaks of CuO can be detected, indicating all CuO in the catalysts reduced to Cu. The intensity of diffraction peaks of Cu for reduced CZA<sub>7</sub>H catalyst decrease significantly, compared to the corresponding peaks for CZA<sub>0</sub>H catalyst. Furthermore, the grain size of Cu decreased significantly for CZA<sub>7</sub>H catalyst. As shown in Table 3, and the grain sizes of Cu ( $d_{\text{Cu}}$ ) which calculated by Scherrer's equation for reduced CZA<sub>0</sub>H and CZA<sub>7</sub>H are 21.4 nm and 9.7 nm, respectively. These results suggest that the addition of Al<sub>2</sub>O<sub>3</sub> can effectively inhibit the Cu crystals growth.

The BET Surface areas ( $S_{\text{BET}}$ ) and the calculated average pore diameter of the catalysts are also listed in Table 3. The  $S_{\text{BET}}$  of the catalysts approximately increases from  $131.7 \text{ m}^2 \text{ g}^{-1}$  to  $161.2 \text{ m}^2 \text{ g}^{-1}$  with the increasing of Al<sub>2</sub>O<sub>3</sub> contents (from CZA<sub>0</sub>H to CZA<sub>7</sub>H), then sharply decreases to  $143.5 \text{ m}^2 \text{ g}^{-1}$  when the Al<sub>2</sub>O<sub>3</sub> contents continuing increasing (CZA<sub>10</sub>H). The variation trend of the micropore volumes is the same as the  $S_{\text{BET}}$  while the trend of average pore diameter of the catalysts is contrary to the  $S_{\text{BET}}$

generally. These results illustrate that the pore structure of the hybrid catalysts can be changed by the introduction of Al<sub>2</sub>O<sub>3</sub>. Meanwhile, a maximum  $S_{\text{BET}}$  of  $161.2 \text{ m}^2 \text{ g}^{-1}$  and a minimum average pore diameter of 6.8 nm are detected for the CZA<sub>7</sub>H catalyst which possesses the smallest grain sizes of Cu ( $d_{\text{Cu}}$ ), as determined from XRD. The result revealed that why the catalyst of CZA<sub>7</sub>H exhibited the maximum of the CO<sub>2</sub> conversion, the DME selectivity and the DME yield simultaneously.

### 3.5 The reducibility of the catalysts

TPR measurements were carried out in order to evaluate the reduction behavior of all the catalysts. Fig. 6 shows the H<sub>2</sub>-TPR profiles of the CZA<sub>x</sub>H catalysts with different Al<sub>2</sub>O<sub>3</sub> contents. It can be found only a single reduction peak with any satellite peaks for all the catalysts. The result illustrate the opinion the copper oxides on the CZA<sub>x</sub>H catalysts are easy to be reduced.<sup>37</sup> Since ZnO and Al<sub>2</sub>O<sub>3</sub> cannot be reduced under the experimental condition, the single high temperature reduction peak can be ascribed to the reduction of CuO species with strongly interaction with ZnO and Al<sub>2</sub>O<sub>3</sub>.<sup>38</sup> With Al<sub>2</sub>O<sub>3</sub> content increasing, the reduction peak maximum firstly shifted towards higher temperature from CZA<sub>0</sub>H to CZA<sub>7</sub>H catalysts, and then shifted towards lower temperature for CZA<sub>10</sub>H, as shown in Fig. 6. The CZA<sub>7</sub>H catalyst possessed the highest reduction temperature at  $373^\circ \text{C}$ , which indicated the strongest interaction between the

Table 3 Physicochemical properties of the CZA<sub>y</sub>H hybrid catalysts

Catalyst	$S_{\text{BET}}/(\text{m}^2 \text{ g}^{-1})$	$V_1$ (Micropore volume)/(cm <sup>3</sup> g <sup>-1</sup> )	$D$ (Average pore diameter)/nm	$d_{\text{CuO}}^a/\text{nm}$	$d_{\text{Cu}}^a/\text{nm}$	$d_{\text{ZnO}}^a/\text{nm}$
CZA <sub>0</sub> H	131.7	0.032	8.0	20.4	21.4	29.1
CZA <sub>1</sub> H	132.1	0.024	8.7	15.4	—	17.6
CZA <sub>3</sub> H	133.4	0.028	7.7	14.4	—	16.5
CZA <sub>5</sub> H	134.1	0.031	7.6	11.4	—	14.1
CZA <sub>7</sub> H	161.2	0.037	6.8	10.9	9.7	13.4
CZA <sub>10</sub> H	143.5	0.030	7.6	10.6	—	12.3

<sup>a</sup> Determined by Scherrer's equation.



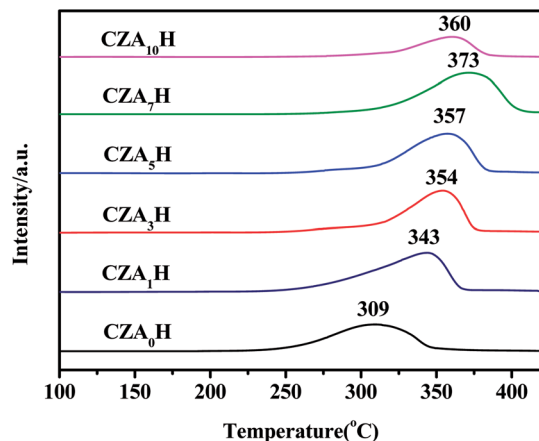


Fig. 6  $\text{H}_2$ -TPR profiles of the  $\text{CZA}_y\text{H}$  hybrid catalysts.

Table 4 The reduction peak areas of the  $\text{CZA}_y\text{H}$  hybrid catalysts

Catalyst	$\text{CZA}_0\text{H}$	$\text{CZA}_1\text{H}$	$\text{CZA}_3\text{H}$	$\text{CZA}_5\text{H}$	$\text{CZA}_7\text{H}$	$\text{CZA}_{10}\text{H}$
Peak area	25 065	30 247	26 320	32 048	38 894	15 425

heterogeneous CuO particles with metal oxides. The  $\text{CZA}_7\text{H}$  catalyst exhibited the best catalytic performance which might be explained that strongly interaction between CuO and oxides was beneficial to  $\text{CO}_2$  hydrogenation to DME.<sup>39</sup> Meanwhile, the  $\text{CZA}_7\text{H}$  catalyst possessed the largest area among the reducing peaks, which revealed that the hydrogen consumption of the catalyst was enhanced significantly, as shown in Table 4. The result implied the largest amount of easily reducible well-dispersed copper oxide existed, which might also be ascribed to the improving dispersion of the CuO particles.<sup>40</sup> This may be one reason why when increase  $\text{Al}_2\text{O}_3$  contents in the catalysts from  $\text{CZA}_0\text{H}$  to  $\text{CZA}_7\text{H}$ , the conversion and selectivity significantly increased and a further increase in  $\text{Al}_2\text{O}_3$  contents adversely influenced conversion and selectivity simultaneously.

### 3.6 Surface acidity of the $\text{CuO-ZnO-Al}_2\text{O}_3/\text{HZSM-5}$ catalysts

Fig. 7 shows  $\text{NH}_3$ -TPD profiles of the  $\text{CZA}_x\text{H}$  catalysts with different  $\text{Al}_2\text{O}_3$  contents. It can be found three  $\text{NH}_3$  desorption peaks which located in the range of 50–200 °C (denoted as peak  $\alpha$ ), 200–350 °C (denoted as peak  $\beta$ ), and 350–600 °C (denoted as peak  $\gamma$ ), respectively. The  $\alpha$ ,  $\beta$  and  $\gamma$  peaks were attributed to weak, medium and strong acid sites, respectively, indicating the presence of three strength acid sites on the hybrid catalysts.<sup>33</sup> The intensity of the low-temperature peak  $\alpha$  of weak acid sites firstly increased with increasing  $\text{Al}_2\text{O}_3$  contents (from  $\text{CZA}_0\text{H}$  to  $\text{CZA}_7\text{H}$ ) and then declined with further increasing  $\text{Al}_2\text{O}_3$  additive, which was agreement with the trend of  $S_{\text{BET}}$  and  $\text{H}_2$ -TPR. The  $\text{CZA}_7\text{H}$  catalyst of the highest peak intensity possessed the largest amount of weak acid sites which were beneficial for methanol dehydration to DME at low temperatures.<sup>24</sup> This might be ascribed to the fact  $\text{Al}_2\text{O}_3$  owned weak acidic characters. In addition, the intensity and the position of the peaks

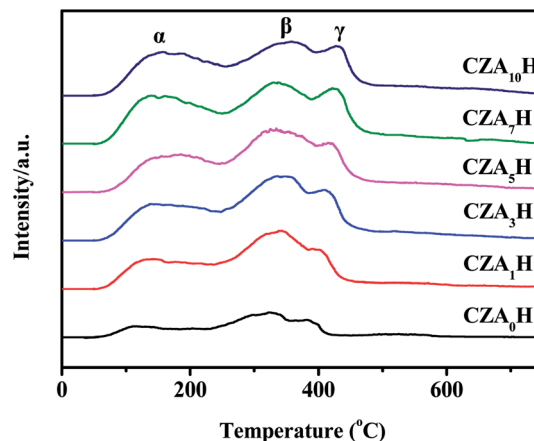


Fig. 7  $\text{NH}_3$ -TPD profiles of the  $\text{CZA}_y\text{H}$  hybrid catalysts.

$\beta$  exhibited unobvious changes with doping different  $\text{Al}_2\text{O}_3$  contents, implying that the strength and amount of medium acid sites cannot be influenced by  $\text{Al}_2\text{O}_3$  additive substantially. The position of peaks  $\gamma$  shifted towards higher temperature gradually, indicating the intensity of strong acid sites increased with increasing  $\text{Al}_2\text{O}_3$  doping, leading to the increase of hydrocarbons in the products. This might be attributed to the fact that the HZSM-5 with possessed strong acid sites could be modified by more oxalic acid with the addition of the more  $\text{Al}_2\text{O}_3$  contents, during the preparation of hybrid catalysts by the co-precipitation method.<sup>11,34</sup> From the above, the amount of weak acid sites enhanced with optimal  $\text{Al}_2\text{O}_3$  modified, which was in favor of obtaining the highest catalytic performance for one-step DME synthesis reaction.<sup>24</sup>

### 3.7 XPS analysis

The XPS spectra of reduced catalysts are shown in Fig. 8. Both of the spectra contained two peaks at about 1022 and 1045 eV (Fig. 8a), which were assigned to Zn  $2p_{3/2}$  and Zn  $2p_{1/2}$  peaks of ZnO, respectively, with a spin energy separation of 23 eV.<sup>41</sup> This illustrates that the Zn atoms are in a completely oxidized state and were not reduced.<sup>42</sup> It can be observed a single peak centered at near 74.2 eV in Fig. 8b, which was attributed to Al  $2p_{3/2}$  of  $\text{Al}_2\text{O}_3$ , therefore, the form of Al was  $\text{Al}_2\text{O}_3$ . Fig. 8c showed the XPS spectra of the Cu 2p for the reduced  $\text{CZA}_0\text{H}$  and  $\text{CZA}_7\text{H}$  catalysts. Two reduced catalysts displayed Cu  $2p_{3/2}$  and Cu  $2p_{1/2}$  main characteristics peaks with binding energy (BE) values of approximately 932.6 eV and 952.6 eV, respectively, with a Cu 2p core level split spin-orbit components ( $\Delta\text{Cu } 2p$ ) of 20.0 eV. The shake-up satellite peaks between 940 eV and 945 eV were not detected, which illustrates the absence of  $\text{Cu}^{2+}$  species in both  $\text{CZA}_0\text{H}$  and  $\text{CZA}_7\text{H}$  catalysts can be reduced to  $\text{Cu}^+$  and/or  $\text{Cu}^0$  species completely.<sup>43,44</sup> Meanwhile, the binding energy (BE) of Cu  $2p_{3/2}$  and Cu  $2p_{1/2}$  for reduced  $\text{CZA}_7\text{H}$  can be observed slightly shifted towards lower BE values, which revealed an enhancement on the interaction between Cu and ZnO with the increasing  $\text{Al}_2\text{O}_3$  contents.<sup>45</sup> The result indicated an influence on Cu chemical combination state due to the increase of the outer-shell electron density of Cu as a consequence of the introduction of additive  $\text{Al}_2\text{O}_3$ . Liu *et al.* thought that the



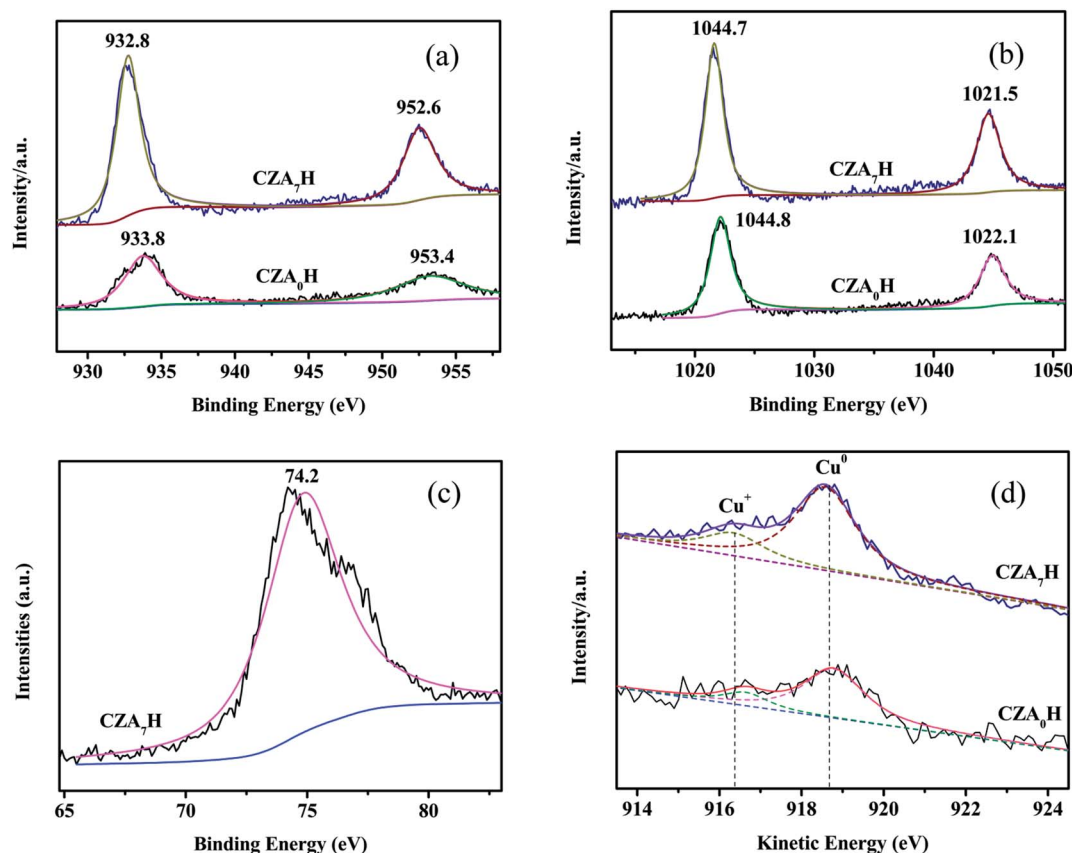


Fig. 8 Spectra of the reduced CZA<sub>0</sub>H and CZA<sub>7</sub>H hybrid catalysts: (a) Cu 2p; (b) Zn 2p; (c) Al 2p; (d) Cu (LMM) Auger.

chemical state of Cu was tightly related to the catalysts performance for CO<sub>2</sub> hydrogenation to DME.<sup>46</sup> This point might be one reason answerable for doping Al<sub>2</sub>O<sub>3</sub> affect the activity of the hybrid catalysts. To distinguish Cu<sup>+</sup> and Cu<sup>0</sup> species, the kinetic energies (KE) of the Cu LMM X-ray auger electron spectroscopy (XAES) spectrum are measured. As shown in Fig. 8d, a broad and asymmetric peak was divided into two peaks, which centered at near 916.5 and 918.7 eV for both reduced CZA<sub>0</sub>H and CZA<sub>7</sub>H catalysts. The two symmetrical peaks are corresponding to the Cu<sup>+</sup> and Cu<sup>0</sup> species, respectively. The line position in the Cu LMM Auger electron spectrum of the two reduced catalysts illustrated that the Cu<sup>0</sup> was the predominant copper species on the CZA<sub>0</sub>H and CZA<sub>7</sub>H catalysts surface. Furthermore, the Cu<sup>0</sup>/Cu<sup>+</sup> area ratios of the two reduced catalysts were calculated based on the corresponding Cu LMM peaks. The area ratio of the reduced CZA<sub>7</sub>H catalyst is a bit higher than that of the CZA<sub>0</sub>H catalyst, which indicated that Cu<sup>0</sup> species but not Cu<sup>+</sup> species might in charge of the activity of these catalysts.<sup>47</sup> The result might be another reason responsible for the improvement in catalytic performance for the Al<sub>2</sub>O<sub>3</sub>-modified hybrid catalysts.<sup>48,49</sup>

## 4. Conclusions

The work discussed the effect of the amount of Al<sub>2</sub>O<sub>3</sub> additive of the CuO-ZnO-Al<sub>2</sub>O<sub>3</sub>/HZSM-5 catalysts on the physicochemical

properties and catalytic performance of the hybrid catalysts based on the optimizing Cu/Zn ratio. The hybrid catalysts for the reaction of CO<sub>2</sub> directly hydrogenation to DME improved the CuO dispersion, reduced the CuO crystallite size, decreased the grain size of the Cu, enhanced the BET surface areas, increased the interaction between the CuO and ZnO, enhanced the amount of weak acid sites, changed the copper chemical state on the catalysts surface and enhanced the catalytic activity and stability with the introduction of the Al<sub>2</sub>O<sub>3</sub> contents. In addition, the influence of the reaction temperature and the space velocity on the catalytic performance of the catalysts modified by Al<sub>2</sub>O<sub>3</sub> was also investigated. The optimal Al<sub>2</sub>O<sub>3</sub> contents (Al<sub>2</sub>O<sub>3</sub> : CuO-ZnO-Al<sub>2</sub>O<sub>3</sub> wt%) of the CuO-ZnO-Al<sub>2</sub>O<sub>3</sub>/HZSM-5 catalysts was 7.0 wt% under the proper Cu/Zn ratio of 7 : 3. The CZA<sub>7</sub>H catalyst for CO<sub>2</sub> hydrogenation to DME showed the maximum CO<sub>2</sub> conversion, DME selectivity and DME yield of 27.3%, 67.1% and 18.3%, respectively, under the reaction conditions of the optimal reaction temperature 260 °C, the appropriate space velocity of GHSV 1500 h<sup>-1</sup> and the conventional pressure of 3.0 MPa.

## Conflicts of interest

There are no conflicts to declare.



## Acknowledgements

This work has been supported by National Nature Science Foundation of China (51301114, 21203125, 51602206), Natural Science Foundation of Liaoning Province (201602598, 2015020649), Science research Foundation of Education Department of Liaoning Province (LQ2017011, L2016003).

## References

- 1 T. Witoon, T. Permsirivanich, N. Kanjanasoonorn, C. Akkaraphataworn, A. Seubsai, K. Faungnawakij, C. Warakulwit, M. Chareonpanich and J. Limtrakul, *Catal. Sci. Technol.*, 2015, **5**, 2347–2357.
- 2 T. Phongamwong, U. Chantaprasertporn, T. Witoon, T. Numpilai, Y. Poo-arporn, W. Limphirath, W. Donphai, P. Dittanet, M. Chareonpanich and J. Limtrakul, *Chem. Eng. J.*, 2017, **316**, 692–703.
- 3 T. Witoon, N. Kachaban, W. Donphai, P. Kidkhunthod, K. Faungnawakij, M. Chareonpanich and J. Limtrakul, *Energy Convers. Manage.*, 2016, **118**, 21–31.
- 4 T. Witoon, S. Bumrungsalee, M. Chareonpanich and J. Limtrakul, *Energy Convers. Manage.*, 2015, **103**, 886–894.
- 5 K. H. Sun, Z. G. Fan, J. Y. Ye, J. M. Yan, Q. F. Ge, Y. N. Li, W. J. He, W. M. Yang and C. J. Liu, *Journal of CO<sub>2</sub> Utilization*, 2015, **12**, 1–6.
- 6 R. J. da Silva, A. F. Pimentel, R. S. Monteiro and C. J. A. Mota, *Journal of CO<sub>2</sub> Utilization*, 2016, **15**, 83–88.
- 7 G. Bonura, C. Cannilla, L. Frusteri, A. Mezzapica and F. Frusteri, *Catal. Today*, 2017, **281**, 337–344.
- 8 Y. Suwannapichat, T. Numpilai, N. Chanlek, K. Faungnawakij, M. Chareonpanich, J. Limtrakul and T. Witoon, *Energy Convers. Manage.*, 2018, **159**, 20–29.
- 9 Y. X. Hua, X. M. Guo, D. S. Mao, G. Z. Lu, G. L. Rempel and F. T. T. Ng, *Appl. Catal., A*, 2017, **540**, 68–74.
- 10 R. Liu, H. F. Tian, A. M. Yang, F. Zha, J. Ding and Y. Chang, *Appl. Surf. Sci.*, 2015, **345**, 1–9.
- 11 D. S. Mao, J. C. Xia, B. Zhang and G. Z. Lu, *Energy Convers. Manage.*, 2010, **51**, 1134–1139.
- 12 G. X. Jia, Y. S. Tan and Y. Z. Han, *Ind. Eng. Chem. Res.*, 2006, **45**, 1152–1159.
- 13 R. Vakili, H. Rahmanifard, P. Maroufi, R. Eslamloueyan and M. R. Rahimpour, *Int. J. Hydrogen Energy*, 2011, **36**, 4354–4365.
- 14 W. G. Gao, H. Wang, Y. H. Wang, W. Guo and M. Y. Jia, *J. Rare Earths*, 2013, **31**, 470–476.
- 15 A. García-Trenco and A. Martínez, *Appl. Catal., A*, 2015, **493**, 40–49.
- 16 T. Witoon, P. Kidkhunthod, M. Chareonpanich and J. Limtrakul, *Chem. Eng. J.*, 2018, **348**, 713–722.
- 17 A. Ateka, I. Sierra, J. Erenia, J. Bilbao and A. T. Aguayo, *Fuel Process. Technol.*, 2016, **152**, 34–45.
- 18 X. H. Zhou, T. M. Su, Y. X. Jiang, Z. Z. Qin, H. B. Ji and Z. H. Guo, *Chem. Eng. Sci.*, 2016, **153**, 10–20.
- 19 A. García-Trenco and A. Martínez, *Appl. Catal., A*, 2012, **411–412**, 170–179.
- 20 S. Wang, D. S. Mao, X. M. Guo, G. S. Wu and G. Z. Lu, *Catal. Commun.*, 2009, **10**, 1367–1370.
- 21 T. Takeguchi, K. Yanagisawa, T. Inui and M. Inoue, *Appl. Catal., A*, 2000, **192**, 201–209.
- 22 V. Vishwanathan, K. W. Jun, J. W. Kim and H. S. Roh, *Appl. Catal., A*, 2004, **276**, 251–255.
- 23 M. Xu, J. H. Lunsford, D. W. Goodman and A. Bhattacharyya, *Appl. Catal., A*, 1997, **149**, 289–301.
- 24 Y. J. Lee, M. H. Jung, J. B. Lee, K. E. Jeong, H. S. Roh, Y. W. Suh and J. W. Bae, *Catal. Today*, 2013, **228**, 175–182.
- 25 J. Xiao, D. S. Mao, X. M. Guo and J. Yu, *Appl. Surf. Sci.*, 2015, **338**, 146–153.
- 26 J. Toyira, M. Saitob, I. Yamauchic, S. Luo, J. Wua, I. Takaharab and M. Takeuchid, *Catal. Today*, 1998, **45**, 245–250.
- 27 H. Lei, Z. Y. Hou and J. W. Xie, *Fuel*, 2016, **164**, 191–198.
- 28 S. Allahyari, M. Haghighi, A. Ebadi and H. Saeedi, *J. Power Sources*, 2014, **272**, 929–939.
- 29 M. Bowker, R. A. Hadden, H. Houghton, J. N. K. Hyland and K. C. Waugh, *J. Catal.*, 1988, **109**, 263–273.
- 30 F. Arena, G. Italiano, K. Barbera, S. Bordiga, G. Bonura, L. Spadaro and F. Frusteri, *Appl. Catal., A*, 2008, **350**, 16–23.
- 31 Y. J. Zhang, D. B. Li, S. J. Zhang, K. J. Wang and J. Wu, *RSC Adv.*, 2014, **4**, 16391–16396.
- 32 Y. J. Zhang, Y. Zhang, F. Ding, K. J. Wang, X. L. Wang, B. J. Ren and J. Wu, *Chem. Ind. Chem. Eng. Q.*, 2017, **23**, 49–56.
- 33 G. Bonura, M. Cordaro, L. Spadaro, C. Cannilla, F. Arena and F. Frusteri, *Appl. Catal., B*, 2013, **140–141**, 16–24.
- 34 L. Y. Li, D. S. Mao, J. Xiao, L. Li, X. M. Guo and J. Yu, *Chem. Eng. Res. Des.*, 2016, **111**, 100–108.
- 35 M. Shimokawabe, H. Asakawa and N. Takezawa, *Appl. Catal.*, 1990, **59**, 45–58.
- 36 L. Shi, C. Y. Zeng, T. J. Wang and N. Tubaki, *Catal. Sci. Technol.*, 2012, **2**, 2569–2577.
- 37 P. S. Sai Prasad, J. W. Bae, S. H. Kang, Y. J. Lee and K. W. Jun, *Fuel Process. Technol.*, 2008, **89**, 1281–1286.
- 38 X. M. Guo, D. S. Mao, G. Z. Lu, S. Wang and G. S. Wu, *J. Catal.*, 2010, **271**, 178–185.
- 39 L. P. Cui, T. Zhou, N. Li, Z. H. Gao, Z. J. Zuo and W. Huang, *Catal. Lett.*, 2017, **147**, 2023–2027.
- 40 Y. J. Zhang, D. B. Li, Y. Zhang, Y. Cao, S. J. Zhang, K. J. Wang, F. Ding and J. Wu, *Catal. Commun.*, 2014, **55**, 49–52.
- 41 O. Lupan, G. A. Emelchenko, V. V. Ursaki, G. Chai, A. N. Redkin, A. N. Gruzintsev, I. M. Tiginyanu, L. Chow, L. K. Ono, B. Roldan Cuenya, H. Heinrich and E. E. Yakimov, *Mater. Res. Bull.*, 2010, **45**, 1026–1032.
- 42 R. Al-Gaashani, S. Radiman, A. R. Daud, N. Tabet and Y. Al-Douri, *Ceram. Int.*, 2013, **39**, 2283–2292.
- 43 Y. H. Wang, W. G. Gao, H. Wang, Y. E. Zheng, W. Na and K. Z. Li, *RSC Adv.*, 2017, **7**, 8709–8717.
- 44 Z. Q. Wang, Z. N. Xu, S. Y. Peng, M. J. Zhang, G. Lu, Q. S. Chen, Y. M. Chen and G. C. Guo, *ACS Catal.*, 2015, **5**, 4255–4259.
- 45 Y. J. Zhao, B. Shan, Y. Wang, J. H. Zhou, S. P. Wang and X. B. Ma, *Ind. Eng. Chem. Res.*, 2018, **57**, 4526–4534.





- 46 R. W. Liu, Z. Z. Qin, H. B. Ji and T. M. Su, *Ind. Eng. Chem. Res.*, 2013, **52**, 16648–16655.
- 47 P. Gao, L. S. Zhong, L. N. Zhang, H. Wang, N. Zhao, W. Wei and Y. H. Sun, *Catal. Sci. Technol.*, 2015, **5**, 4365–4377.
- 48 B. Xue, L. Hui, H. Q. Yang, Y. L. Zhao, L. X. Hou and W. Li, *Ind. Eng. Chem. Res.*, 2017, **56**, 135–142.
- 49 Y. J. Zhang, N. Zheng, K. J. Wang, S. J. Zhang and J. Wu, *J. Nanomater.*, 2013, **7**, 246–247.

